# High Current Ion Source Development at Frankfurt

**K. Volk, H. Klein, A. Lakatos, A. Maaser, M. Weber**
**Institut für Angewandte Physik, Universität Frankfurt**

## I. Introduction

The development of high current positive and negative ion sources is an essential issue for the next generation of high current linear accelerators. Especially, the design of the European Spallation Source facility (ESS) and the International Fusion Material Irradiation Test Facility (IFMIF) have increased the significance of high brightness hydrogen and deuterium sources. As an example, for the ESS facility, two $H^-$-sources each delivering a 70 mA $H^-$-beam in 1.45 ms pulses at a repetition rate of 50 Hz are necessary [1]. A low emittance ($\varepsilon_{rms,norm} \sim 0.1\pi$ mmmrad) is another important prerequisite. The source must operate, while meeting the performance requirements, with a constancy and reliability over an acceptable period of time. The present paper summarizes the progress achieved in ion sources development of intense, single charge, positive and negative ion beams.

## II. Experimental setup

### A. Description of the HIgh EFficiency Source

The **HI**gh **EF**ficiency Source (HIEFS) [2] is a compact high brilliance ion source designed to supply intense ion beams. It was optimized to generate nearly pure atomic ion beams with a single charge state only (e.g. $He^+$, $N^+$, $O^+$, $Ar^+$). By using Helium (Nitrogen) as operation gas, the 80% normalized 4rms-emittance was measured to $0.003\pi$ mmmrad ($0.01\pi$ mmmrad), which corresponds to an ion temperature of 300 K (1480 K) only [3]. A schematic cross-sectional view of the HIEFS and the extractor is shown in Fig. 1. The plasma generator is made of a water-cooled cylindrical copper chamber whose dimensions are 6.0 cm in diameter by 10.5 cm depth. In the middle of the chamber, a tungsten cathode (1.8 mm diameter) is mounted. The front-end of the chamber is closed by the plasma electrode, which can be biased with respect to the anode. This arrangement serves to control the plasma potential near the plasma electrode. On the backside are the gas inlet and several rows of permanent magnets in cuspfield arrangement to reduce particle losses. A solenoid is surrounding the plasma chamber to confine the plasma in longitudinal direction ($B_z$). Near the plasma electrode an electro-magnet is installed as a filter, forming a transverse magnetic field ($B_y$) with a magnitude of about 100 G at axis.

For ion extraction, a single aperture accel-decel-system is used, designed for beam energies up to 30 keV. The diameter of the outlet aperture is variable from 3 mm to 8 mm. The distance between outlet and screening electrode is 6 mm. The screening electrode is on a negative potential of up to 3 kV with respect to the ground electrode and serves as a barrier for secondary electrons from the beam line. In case of negative ion extraction, the electron beam is deflected outside of the beam channel by means of the filter magnet field distribution in the extraction region. That way, the electrons are dumped on the screening electrode. All measurements were performed with the source and extraction system operated in dc-mode.

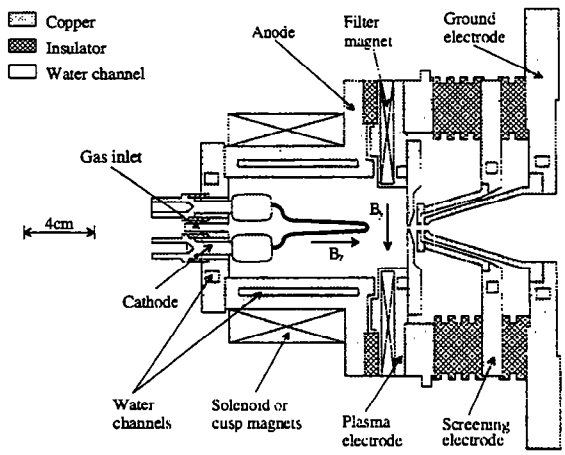


*Fig. 1 Schematic drawing of the HIEFS.*

### B. Description of the $H^-$-source

Based on the experimental results with the HIEFS, a more optimized version was built [4]. A schematic drawing of the this source is shown in Fig. 2. The source can be divided into three parts: the plasma generator, the extraction system and the dumping system. Because of the high heat conductivity, the discharge chamber is made of a water-cooled copper cylinder (12 cm depth, 10 cm diameter). For high reliability the plasma generation is done by rf drive. A high reliability and little fluctuations are essential to ensure a constant current from pulse to pulse. The rf-coupling

inductor is positioned on the cylinder axis. To optimize its z-position the antenna is movable. For the experiments transmitter from 1.7 to 27 MHz with up to 100 kW are available. This allows us to investigate the source at different frequencies. At the beginning the source will be driven without cesium. Later on cesium will be injected to enhance the $H^-$ yield. Like the HIEFS, the plasma generator is equipped with a solenoid, cusp magnets on the back wall and a filter magnet on the front end.

For the ion beam formation a single aperture accel-decel system is used. The distance between the outlet aperture and the screening electrode is 7 mm, the extraction voltage up to 35 kV. The radius of the outlet aperture is a compromise to guarantee low gas flow and low beam emittance as well as a large ion current. For higher beam energies a 60 kV / 300 mA power supply is being ordered.

In this version of source, a dumping system will be used to dump the electrons. It consists of a bending magnet (mounted in the screening electrode) and a water cooled dumping tube. By means of the transverse magnetic field, the electrons will be deflected (40°) outside the $H^-$-beam. In the electric field between the screening electrode and the dumping tube, the electron beam will be decelerated to few kV and finally annihilate in the tube.

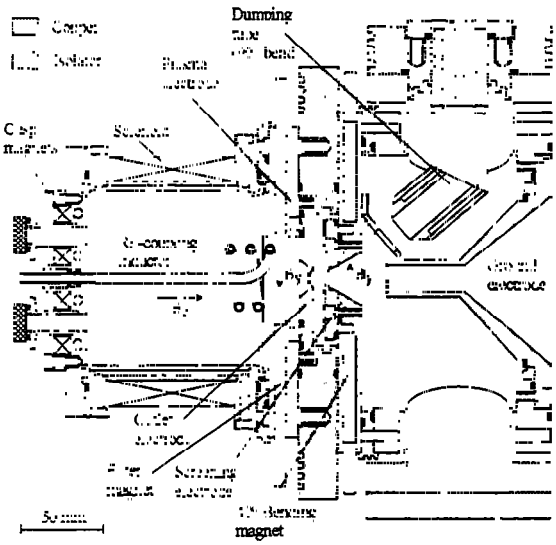


*Fig. 2 Schematic drawing of the $H^-$-source.*

### C. Description of the test stand

An experimental setup is depicted in Fig. 3. The beam diagnostics consist of a faraday cup, an emittance measurement device and a bending magnet to analyze the beam composition. The whole facility is placed in a vacuum chamber.

The moveable water-cooled high current faraday cup was designed for a maximum power density of 1 kW/cm$^2$. It is fabricated from stainless steal and equipped with a repeller electrode. The emittance measurement device works according to the slit grid principle. Due to the high beam power density, a new water cooled slit was built. Slit and grid are computer-controlled driven through the beam independently by stepping motors. Because of the quantization error of the emittance device, one has to use as high resolution as possible [5]. The maximum linear resolution is given by the slit height, in our case 0.1 mm. To increase the angular resolution, the feedthroughs for the slit and grid are mounted in different vacuum chambers. This allows to increase the slit-grid distance, and so the angular resolution as far as the full beam just hit the grid. Behind the slit, an electrostatic deflection system is installed. To determine the pure $H^-$-beam emittance, we take away the $H^0$-beam emittance from the full beam emittance ($H^0$ + $H^-$) numerically. The pure $H^0$-beam emittance will be measured by deflection of the $H^-$-beam between the slit and the grid. At the exit of the emittance measurement device a 75° bending magnet is installed to analyze the ion distribution.

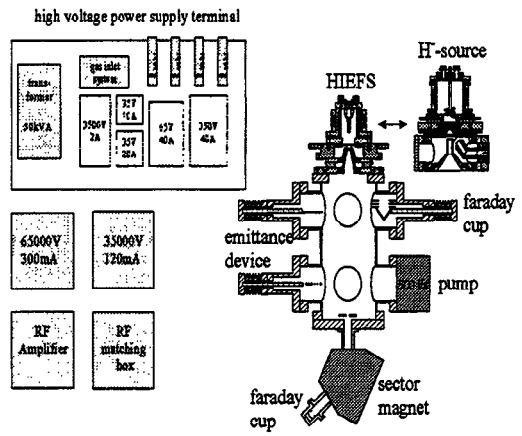


*Fig. 3 Schematic drawing of the experimental setup.*

## III. Experimental results

### A. Operation with $H^-$

Negative ion extraction is always accompanied by the extraction of electrons. According to the Child-Langmuir law, the space charge of the extracted electrons reduces the extractable $H^-$-current. Consequently, for a given design current, the diameter of the outlet aperture has to be larger than for an extraction without electrons. This leads to a higher gas flow in the extractor, accompanied

by a higher rate of recombination, charge transfer and stripping of the extracted $H^-$-ions. Furthermore, the electron beam has to be dumped and the beam power has to be deposited in the extractor. Therefore, a low electron to $H^-$-ratio is essential for negative ion extraction. In order to determine the optimum conditions for generating high current $H^-$-beams with a low electron to $H^-$-ratio, the influence of the plasma parameter on the electron to $H^-$-ratio and the current density were investigated.

We assumed that the relative position of the arc discharge with respect to the filter field might have an influence on the electron to $H^-$-ratio. First of all, the polarity of the cathode was changed as it inverts the direction of the magnetic field that it produces itself. We found significant differences in the electron to $H^-$-ratio and chose the configuration with the better yield for further operation. Then, both the angular position and the cathode length were varied and the effect on the electron to $H^-$-ratio was studied.

The influence of the cathode length on the electron to $H^-$-ratio is depicted in Fig. 4. The larger the distance between cathode and filter field, the better the ratio obtained. The reason is that the fast electrons intersect the magnetic field lines right away. Consequently, their fraction in the extraction region area is diminished. That way, with a cathode length of 10 mm, an electron to $H^-$-ratio of eight was obtained. Additional flanges to enlarge the distance between cathode and filter field are under construction. From these experiments, we expect further improvement in the electron to $H^-$-ratio.

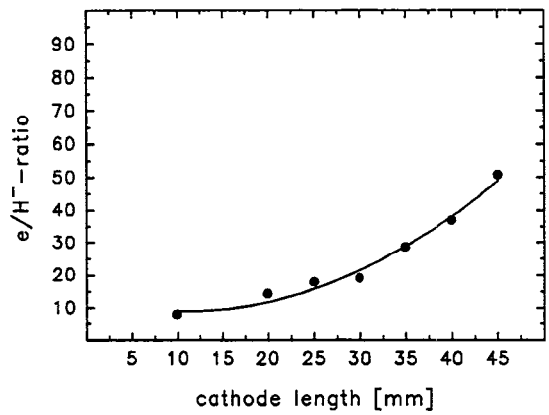


*Fig. 4 Electron to $H^-$-ratio as function of the cathode length.*

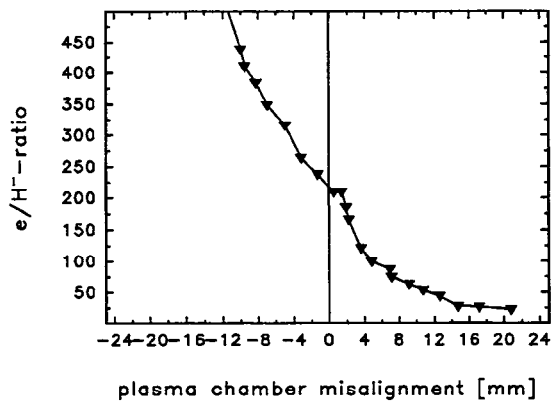


*Fig. 5 Electron to $H^-$-ratio as function of the plasma chamber misalignment.*

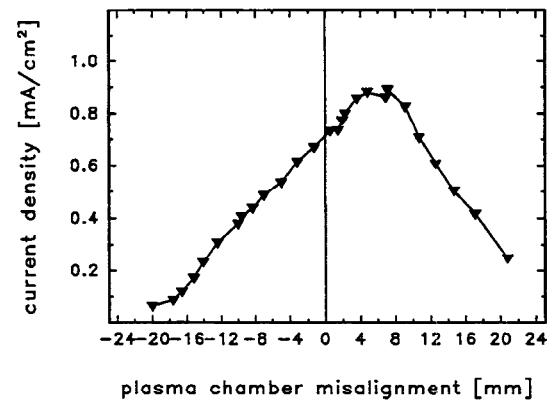


*Fig. 6 $H^-$-current density as function of the plasma chamber misalignment.*

Due to the transverse filter field ($B_y$) and the potential distribution in the plasma column along the z-axis, the plasma column experiences a drift movement perpendicular to the electrical and magnetic field. That way, the center of the plasma column does not agree with the axis of the plasma chamber. Therefore, the electron to $H^-$-ratio and the emission current density as function of the chamber misalignment (resp. the plasma column) were investigated. In Fig. 5 and 6, the results of these experiments are presented. On the x-axis, the distance between the plasma chamber axis and the plasma electrode axis (beam axis) is plotted. The zero-position means a symmetrical alignment of the plasma chamber. As shown in Fig. 5, positioning out of the middle decreases significantly the electron to $H^-$-ratio, while the

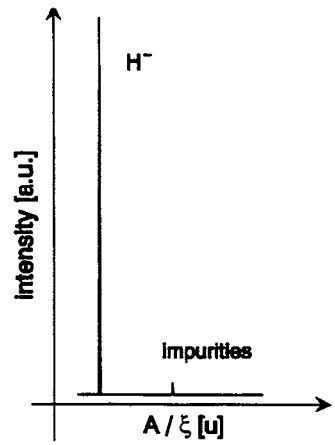


*Fig. 7 $H^-$-spectrum*

extracted current density reaches a maximum, if the misalignment distance is about 7 mm. In that mode of operation, we obtained a current density of 10 mA/cm$^2$ for an arc power as small as 1 kW. Fig. 7 presents a mass spectrum taken at an extraction voltage of 8 kV only. The spectrum shows a 10 mA H$^-$-beam with 1.8% of impurities. Note that we have not used cesium in the plasma chamber so far.

A key problem of negative ion extraction is the simultaneous extraction of ions and electrons. Without an e-dumping system inside the ion source, it is necessary to dump the electrons inside the LEBT or the RFQ, which leads to a higher technical effort.

In case of negative ion extraction the extracted H$^-$-current will be reduced by the space charge of the extracted electrons. In order to calculate the extractable H$^-$-current, the law of Child-Langmuir had to be modified. In Fig. 8 the calculated H$^-$-current is shown under the condition of an extraction voltage of 35 kV and an aspect ratio of 0.357.

The dumping system consists of two parts. In the first part, the beam is decelerated with a designated dumping voltage which depends on the current of the electron beam in the front part of the system. Then, in the back part of the system, the electron beam spreads and will be dumped in the water cooled tube outside of the beam channel. An IGUN simulation [6] of the electron beam course in the dumping system is shown in Fig 9.

In this way, we can use a high perveance extractor. Due to the deceleration of the electron beam, we get low dumping power. Additionally, one achieves a high flexibility in the source handling and a low influence on the H$^-$-beam emittance. The thermal stress of the dumping system material will be about 20 Watt/cm$^2$. This power density can be controlled by a water cooled catcher.

To optimize the electron to H$^-$-ratio and the current density of the plasma generator we use a electrical dipole magnet as filter magnet. To minimize the magnetic field strength at the outlet aperture, the filter magnet and the bending magnet of the dumping system have the opposite polarity. In this way an undesired electron beam deflection in the accelerator gap is reduced and the negative influence of the resulting magnetic field at the plasma sheath is minimized. Fig. 10 shows a high resolution measurement of the resulting $B_y$-field. The negative region corresponds to the plasma chamber (filter magnet), and the positive region to the extractor (bending magnet). As the measurement shows, we get a minimized $B_y$ field strength in the plasma sheath region.

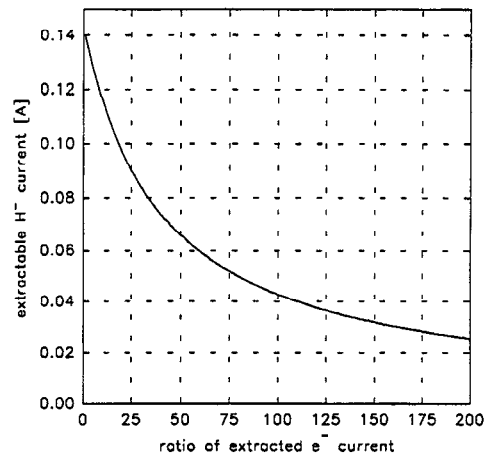


*Fig. 8 Calculated extractable H$^-$-current.*

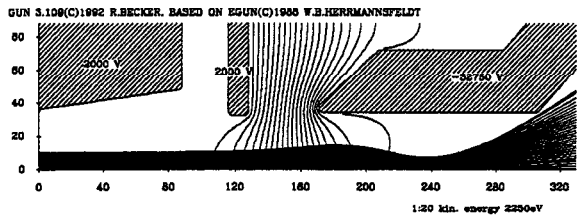


*Fig. 9 Simulation of the dumping system.*

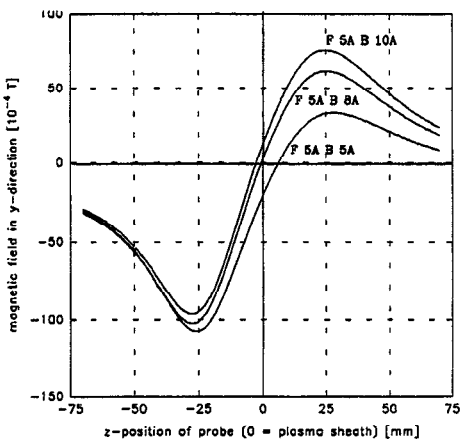


*Fig. 10 $B_y$-field vs. z-position at the axis.*

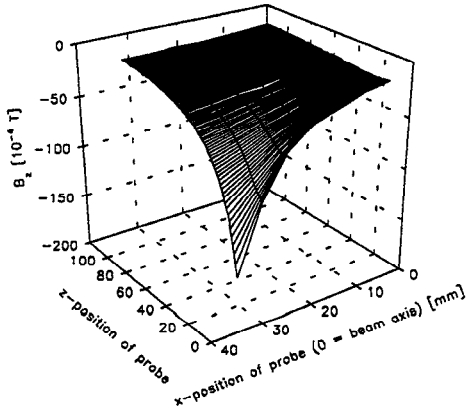


*Fig. 11 $B_y$-field in the dumping region.*

For ion optical calculations, the exact knowledge of the magnetic field course between the plasma sheath to the dumping tube is necessary. As an example, in Fig. 11 the $B_z$-field is shown in the dumping region. The dumping system was built in our workshop and a dumping power supply (3500 V, 2 A) was delivered, a high voltage platform is being built.

## B. Operation with $H_2^+$

The dependence of the extracted ion species on various discharge parameters were investigated to determine the optimal conditions for generating a high percentage of $H_2^+$ ions.

For the ion species percentage of the beam, the gas pressure in the source is an essential parameter. A graph of the ion species percentage in the extracted beam as a function of the gas pressure is shown in Fig. 12. The source is operated with a discharge voltage of 100 V, a discharge current of 1.5 A and a solenoid field of 12 mT. It can be seen that for low gas pressures the $H_2^+$-fraction increases beyond 85 %. At the same time, the $H_3^+$-fraction decreases while the atomic fraction does not change. This dependence is consistent with the known cross-section for $H_3^+$ production (via $H_2^+ + H_2 \Rightarrow H_3^+ + H$), which is the pre-dominant reaction in the plasma chamber. This way, raising the neutral gas pressure leads to an increase of the $H_3^+$- fraction.

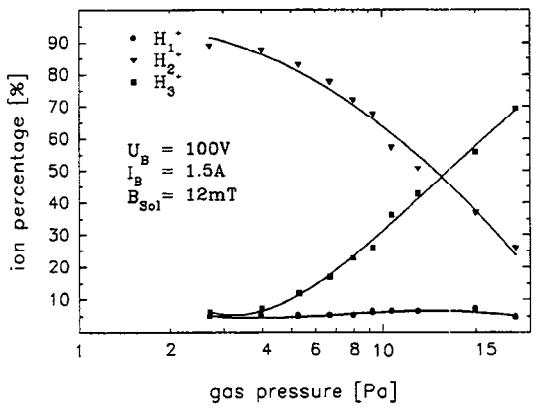


*Fig. 12 Ion species ratio vs. gas pressure.*

It is also observed that the amount of the $H_2^+$-fraction is a function of the arc voltage between cathode and anode. The arc voltage corresponds to the maximum electron energy in the plasma chamber. The result is plotted in Fig. 13 and shows, that for arc voltages in the range of 60 - 100 V the $H_2^+$ ion species percentage yield in a maximum. For higher arc voltages decrease the $H_2^+$-fraction, accompanied by an increase of the $H_3^+$-fraction. The $H_1^+$-percentage remains stable over a wide range. This behavior can be explained by the cross-section for the ionization of molecular hydrogen by electron impact ($e^- + H_2 \Rightarrow H_2^+ + 2e^-$). The cross-section shows, that electron energies between 50-100 eV yield a maximum production of $H_2^+$-ions. This means, that arc voltages, respectively electron energies, higher than 100 V or below 50 V leads to a reduction of the $H_2^+$ fraction. During source operation, arc voltages less then 60 V are impossible because the source does not operate in that range.

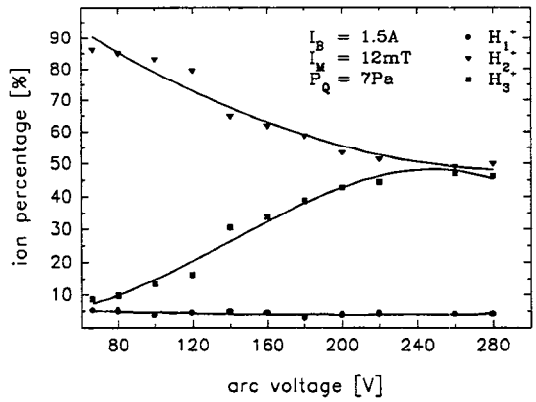


*Fig. 13 Ion species ratio vs. arc voltage.*

Further measurements have shown, that the $H_2^+$-fraction is independent on the arc current. On the other hand, the arc current is an essential parameter to reach high current densities. That way in a next step the source will be optimized for the extraction of high beam currents.

## C. Operation with $D^+$

Usually, deuterium ion beams consist of three species: the atomic $D_1^+$, the molecular $D_2^+$ and $D_3^+$. In order to enhance the atomic yield, the influence of all essential plasma-parameters (including cathode length and position of the magnets) on the beam composition were investigated [7]. The experiments were initially carried out with hydrogen and then continued with deuterium. For identical plasma-parameters, the results of the ion species percentage were basically the same for both gases. In the case of deuterium, the atomic fraction is a few percent higher than for hydrogen. Subsequently, the main results for deuterium will be presented.

Fig. 14 illustrates the relationship between the ion species percentage and the arc current for a constant arc voltage of 55 V and a solenoid field of 24 mT. The source pressure is 9 Pa, and the plasma-electrode is on negative potential of 150 V with respect to the anode. The plot shows, that for high arc currents the atomic fraction exceeds 90 %. On the other hand, the $D_3^+$-fraction decreases while the $D_2^+$-fraction does not change.

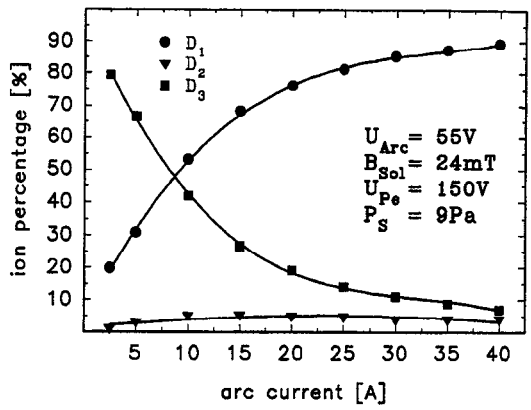


*Fig. 14 Ion species ratio vs. arc current.*

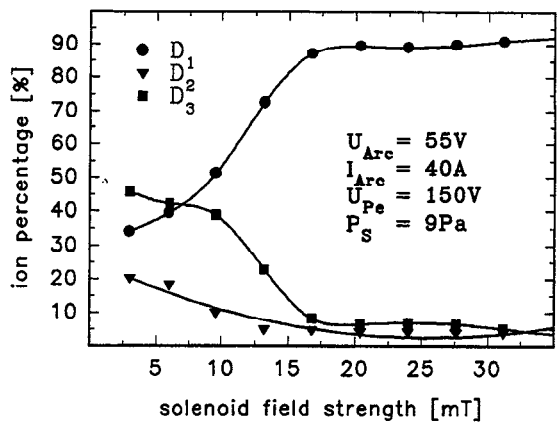


*Fig. 15 Ion species ratio vs. solenoid field strength.*

Furthermore, the atomic fraction is very sensitive to changes in the solenoid field. Only a strong magnetic field in combination with a high discharge power leads to a high percentage of the atomic fraction. According to the plot of the measured ion species percentage versus the magnetic field of the solenoid (Fig. 15), the atomic fraction has dropped for a rising magnetic field to 93 % while the $D_2^+$- and $D_3^+$-concentration has decreased to 4 % and 3 %, respectively.

As mentioned above, a high atomic fraction requires a high discharge power and a strong longitudinal magnetic field. Both parameters lead to a high current density. That way, a maximum emission current density of 210 mA/cm$^2$ has been achieved for a 1.5 mm aperture radius. Operating the source at 35 kV with a 4 mm aperture radius of the plasma electrode delivers 80 mA $D^+$.

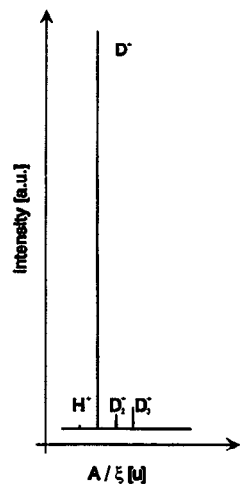


*Fig. 16 $D^+$-Spectrum*

Fig. 16 presents a typical spectrum taken at an arc current of 40 A and a solenoid field of 24 mT. The spectrum shows an atomic fraction of 91 %, 3 % for $D_2^+$ and 5 % for $D_3^+$. The fraction of impurities is about 1 %.

## IV. Acknowledgments

The authors would like to thank G. Hausen and his team for their continued technical support.

## V. References

[1] Klein, H., Linac design for the European Spallation Source, Proc. Int. Conf. on Accelator-Driven Transmutation and Application, Las Vegas, USA (1994)
[2] Volk, K. et. al., A Compact High Brilliance Ion Source For RFQ Injection, Proceedings of EPAC, London, 1438 (1994)
[3] Volk, K., Dissertation Univ. Frankfurt (1993)
[4] Volk, K. et. al., An H$^-$-Source for ESS, Proceedings of the 6th International Conference on Ion Source, Whistler, Canada (1995)
[5] Ludwig, T., Quantization error of slit-grid emittance measurement devices, Proceedings of the 5th International Conference on Ion Source, Peking, China (1993)
[6] Becker, R., Herrmansfeldt W.B., Proceedings of the 4th International Conference on Ion Source, Bensheim, Germany (1991)
[7] Maaser A. et. al., Development of a $D^+$-Source in Frankfurt, Proceedings of the 6th International Conference on Ion Source, Whistler, Canada (1995)